Neurocomputing 74 (2011) 661–670

Contents lists available at ScienceDirect

Neurocomputing

journal homepage: www.elsevier.com/locate/neucom

Image reconstruction by an alternating minimisation

Xiaoqiang Lu [a], Yi Sun [a], Yuan Yuan [b,*]

[a] Department of electrical engineering at Dalian University of Technology, Dalian, P.R. China
[b] Center for OPTical IMagery Analysis and Learning (OPTIMAL), State Key Laboratory of Transient Optics and Photonics, Xi'an Institute of Optics and Precision Mechanics, Chinese Academy of Sciences, Xi'an 710119, Shaanxi, P.R. China

ARTICLE INFO

Article history:
Received 25 April 2010
Received in revised form
28 July 2010
Accepted 11 August 2010
Communicated by Xiaofei He
Available online 25 August 2010

Keywords:
Limited angle tomography
Ill-posed inverse problem
Total variation (TV)

ABSTRACT

This paper focuses on the problem of incomplete data in the applications of the circular cone-beam computed tomography. This problem is frequently encountered in medical imaging sciences and some other industrial imaging systems. For example, it is crucial when the high density region of objects can only be penetrated by X-rays in a limited angular range. As the projection data are only available in an angular range, the above mentioned incomplete data problem can be attributed to the limited angle problem, which is an ill-posed inverse problem. This paper reports a modified total variation minimisation method to reduce the data insufficiency in tomographic imaging. This proposed method is robust and efficient in the task of reconstruction by showing the convergence of the alternating minimisation method. The results demonstrate that this new reconstruction method brings reasonable performance.

1. Introduction

Circular cone-beam computed tomography (CT) has been widely used in industrial non-destructive testing and medical imaging because it involves minimum hardware implementation complexity. Reconstruction from the complete data is well understood, and the conventional and most commonly used method for reconstruction of complete projections is the standard filtered back projection (FBP) reconstruction technique [1].

However, it is not always possible to acquire projection data through a complete angular range in many applications. Some examples would be X-ray dose limitations, or time constraints when imaging a moving object, or X-rays being obstructed when passing through high-density region of objects. In these cases, the projection data can be acquired only from a view angle significantly less than 180°, leading to the limited angle tomography. When data are collected by an actual CT scanner for a small number of projections, as occurs in a number of applications in dental radiology, surgical imaging, thoracic imaging, mammography, etc., this leads to the notorious ill-posed problem. Because the complete set of projections is precondition of constructing "well" image based on FBP, it cannot get "well" image reconstruction from few projection data by using FBP algorithm.

An interesting method to overcome the effects of limited angular range is to develop iterative image reconstruction algorithm. In image reconstructions, iterative reconstruction algorithms have numerous potential advantages over their analytical counterparts in limited angle cases [2]. When the projection data are incomplete, the analytical algorithms result in poor reconstructions with severe artifacts. Much work has been done on developing iterative algorithms to overcome data insufficiency for CT image reconstruction over the past two decades. Many researchers attempted several approaches including statistical method, wavelet technique, algebraic reconstruction methods, the expectataion-maximisation algorithm, variation methods, level set, and many others. For example, Natterer [1] discussed many mathematical aspects for forming reconstructions from limited data, such as uniqueness and stability of solutions. The expectation-maximisation method was given in [3], which was then used to develop a reconstruction algorithm. Kole [4] applied relaxation to three different statistical ordered subset algorithms for image reconstruction in CT. Statistical inversion with *a priori* information for reconstruction in limited angle tomography has also been published [5–8]. Reconstruction algorithm based on wavelet can be found in [9,10]. More promising approaches include algebraic reconstruction were widely used for tomographic imaging [11–13]. Other algorithms on limited angle tomography and further references could be found in [14–18]. Level set methods is introduced for limited angle tomography problem in [19]. The authors presented a novel approach to tomographic reconstruction based on variational framework in [20]. The presented paper describes a new practical approach to the reconstruction problem using a Hopfield-type neural network in [21].

Adaptive wavelet-Galerkin method is introduced by the authors in [34] to solve to the limited angle problem, and the reconstruction strategy has a comparable performance with a significant reduction in computational time.

* Corresponding author.
E-mail address: yuany@opt.ac.cn (Y. Yuan).

0925-2312/$ - see front matter © 2010 Elsevier B.V. All rights reserved.
doi:10.1016/j.neucom.2010.08.003

Because limited angle tomography is actually an incomplete reconstruction with few projection data, its reconstruction is very ill conditioned. A classical method for solving ill-posed problems is regularisation with a quadratic penalty function [35]. However, the quadratic regularisation methods have a tendency of smoothing those sharp edges in solutions that often carry important information. This observation explains an interest in regularisation with non-quadratic penalties which preserves the discontinuities in the solution, the most popular of which is probably the total variation penalty. For the limited angle problem, methods like the total variation in [22] were shown to be very promising. A recent paper by Candès et al. [23] proposed a TV algorithm and proved an impressive result about the possibility of perfect reconstruction, given small amounts of data. Pan et al.[24–26] made a lot of work on image reconstruction from incomplete projections. The authors in [27] present a novel image reconstruction method via minimising the total variation (TV) of the reconstructed image for limited view angle X-ray computed tomography.

This paper intends to make some further contribution to the subject in reconstructing an image from limited angle based on TV minimisation method. We first defined a new objective function by adding the gradient to the new minimisation problem. Then an alternating minimisation algorithm is employed to implement the minimisation problem. We show the convergence of the alternating minimisation algorithm and demonstrate the feasibility of our method by numerical examples using projection data in a limited angular range. In the numerical examples, we found that the quality of reconstructed image by the proposed method is improved compared to the method in [29] and the expectation-maximisation (EM) algorithm.

This paper is organised as follows. In Section 2, we demonstrate discrete data model for circular cone-beam CT. In Section 3, we describe the new optimisation program for the limited angle tomography. Numerical results are presented in Section 5, and conclusions are presented in Section 6.

2. Date model in circular cone-beam CT

In circular cone-beam CT, the task in image reconstruction is to recover the density of an object $f(x)$ under examination provided by a set of line integrals. Consider a coordinate system $\{X,Y,Z\}$ that is fixed on the imaged object. As shown in Fig. 1, the source trajectory can be written in the fixed-coordinate system as

$$\vec{s}(\lambda) = (R\cos\lambda,\ R\sin\lambda,\ 0)^T \tag{1}$$

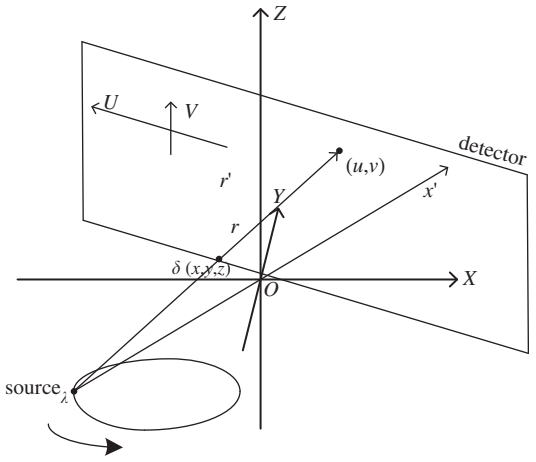

Fig. 1. Cone-beam CT data acquisition geometries.

where λ denotes the rotation of angle of the X-ray source, R denotes the distance from the source point to the rotation axis. The cone-beam projection of the object function $f(x)$ at a point (u,v) on the detector can be expressed as

$$p(u,v,\lambda) = \int_0^\infty f(\vec{s} + t\theta(a,u,v))dt \tag{2}$$

And the ray direction vector $\theta(\lambda,u,v)$ indicates the direction of the ray starting from source point $\vec{s}(\lambda)$ and passing through the point (u,v) on the detector. By discretising the projection acquisition model, Eq. (2) can be approximated by following the discrete linear system:

$$P = kf \tag{3}$$

The projection vector P consists of M-length measured projection data. f is a vector of length N with individual elements f_j, $j = 1,2,\ldots,N$. The system matrix k is a discrete model for the integration in Eq. (1). Hence, the projection acquisition model can be written as a set of linear equations when considering the error of measurement or noise:

$$\sum_{j=1}^{N} k_{ij}f_j + n_i = p_i, \quad i = 1,2,\ldots,M \tag{4}$$

where M is the number of X-ray integrals, N the number of pixels in the object, and $n_i(i = 1,2,\ldots,M)$ is the additive noise associated with the measurement, k_{ij} is system weights which are determined by the intersection length of the ith ray through the jth pixel, and f_j represents the jth pixel value.

3. The optimisation program for limited angle tomography

To simplify notations, the projection acquisition model in Eq. (4) is described by the following formula:

$$P = kf + n \tag{5}$$

where big column vector P is composed of all measured projection data at each view of limited angular range, f is a vector of length N with individual elements $f_j j = 1,2,\ldots,N$, k is composed of every weight k_{ij}. Because limited angle tomography is actually an incomplete reconstruction, formula (5) is an underdetermined system of linear equations. Because some singular values of the singular matrix k converge to zero in underdetermined system of linear equations, the condition number of the matrix is large. For the underdetermined system of linear equations, small change in f can result large change in P. Hence the equations is very ill conditioned. Moreover, M and N are very large and unequal. Introduction of a new method that is simple and effective to solve Eq. (8) would therefore be invaluable.

3.1. Review

In general, the conventional and most commonly used method for solving the ill-posed problems is least-squares method combined with a penalty function. The idea of the method is to find the approximate solution to the following optimisation problem: find f^* that minimises its problem

$$f^* = Q(f) + \lambda c(f) \tag{6}$$

where the data fitting term $Q = \|kf - P\|_2^2$ and c is called the regularizer or regularisation function and λ is a Lagrange multiplier. Since it is much less expensive to compute the gradient $\nabla Q(f)$ [28]. The authors in [29] propose iterative methods by solving an optimisation subproblem involving a quadratic term

with diagonal Hessian plus the original sparsity. The approach is suitable for cases in which this subproblem can be solved much more rapidly than the original problem. The authors in [29] solved problem (6) by generating an iterated sequence $\{f^t, t=0,1,\ldots\}$ and turned problem (6) into the following l_1-norm subproblem:

$$f^{t+1} \in \arg\min_z (z-f^t)^T \nabla Q(f^t) + \frac{\alpha_t}{2}\|z-f^t\|_2^2 + \tau\|z\|_1 \quad (7)$$

where α_t and τ are the non-negative parameter, $\|\cdot\|_1$ denotes the l_1-norm, and z denotes the solution waiting to be solved. The l_1-norm of the image is simply the sum of the absolute values of the image pixel value. Formation (7) can identify sparse approximate solutions to the underdetermined system (5). l_1-norm formation can be accomplished by minimising the l_1-norm of the image constrained by the fact that the image yields the measured projection data. Hence l_1-norm formation can solve efficiently the underdetermined system (5) when the reconstructed image or the reconstructed signal is sparse. Since tomographic images are generally extended distributions and are relatively constant over extended volumes in limited angle tomography, the reconstructed image might not be sparse violating the prerequisite of employing the l_1-norm formulation. However, the image formed by taking the magnitude of its gradient could be approximately sparse [23]. If the pixel values of image are labeled by $z_{s,t}$, the image gradient magnitude is

$$|\nabla z_{s,t}| = \sqrt{(z_{s,t}-z_{s-1,t})^2 + (z_{s,t}-z_{s,t-1})^2} \quad (8)$$

That is, the l_1-norm of the gradient image is known as the total variation (TV) of the image:

$$\|z\|_{TV} = \sum_{s,t} |\nabla z_{s,t}| = \sum_{s,t} \sqrt{(z_{s,t}-z_{s-1,t})^2 + (z_{s,t}-z_{s,t-1})^2} \quad (9)$$

3.2. Formulation of the new method

In general, the effectiveness of the TV-norm formulation relies on the fact that the imaged object has a relatively sparse gradient image. The addition of the TV-norm formulation has a very positive effect on the quality of reconstruction for piecewise smoothness of an unknown image. Hence, we propose a new alternating optimisation program for limited angle tomography by combining the gradient with the TV-norm in this section. The proposed alternating optimisation program is given by

$$z = \arg\min (z-f)^T \nabla H(f) + \tfrac{1}{2}\lambda\|z-f\|_2^2 \quad (10)$$

$$f = \arg\min \tfrac{1}{2}\|z-f\|_2^2 + \mu\|z\|_{TV} \quad (11)$$

where z is a set of images satisfying the data fidelity, $H(f) = 1/2\|kf-P\|_2^2$, $(z-f)^T$ denotes the transpose of $(z-f)$, $\|z\|_{TV} = \sum_{s,t}\sqrt{(z_{s,t}-z_{s-1,t})^2 + (z_{s,t}-z_{s,t-1})^2}$, s and t are the horizontal and vertical position of image z, λ and μ are positive constants. The main difference between Eq. (6) and (10) is that a fitting term $||z-f||_2^2$ and a gradient are added in the new optimisation program. The proposed optimisation program is based on four things: since the matrix k of data model is too large to be handled explicitly, computation of ∇M may be carried out efficiently. The algorithm based on TV is more suitable for limited angle tomography because it can reconstruct sharp discontinuities or edges with sparse or insufficient data that may occur due to practical issues of CT scanning. When the projection data P are incomplete in limited angle tomography, a large set of images may be consistent with the available data. That is, there exists a set of images which satisfy Eq. (10). The minimisation of the TV-norm in Eq. (11) is used to select a unique image from the set of images. It is much less expensive to compute the gradient ∇H and to solve the optimisation program (10), (11) than it is to solve the original problem (5) by other means [29]. Compared to [29], the main advantage of the proposed method is that a TV-norm is used in the image reconstruction process. Therefore, the new method has the ability to preserve edges very well in the reconstruction image.

Proposition 1. *When the matrix $A = -(1/2\lambda)kk^T$ is defined, we have the following identity*:

$$(z-f)^T \nabla H(f) + \tfrac{1}{2}\lambda\|z-f\|_2^2 = (kf-P)^T A(kf-P) \quad (12)$$

Proof. We can derive the following identities:

$$\nabla H(f) = k^T(kf-P) \quad (13)$$

Eq. (14) can be obtained by considering the minimisation of Eq. (10) with respect to z:

$$z = f - \frac{1}{\lambda}\nabla H(f) = f - \frac{1}{\lambda}k^T(kf-P) \quad (14)$$

And Eq. (15) can be obtained by considering Eq. (14) and the second term of Eq. (10) is

$$\frac{\lambda}{2}\|z-f\|_2^2 = \frac{1}{2\lambda}(kf-P)^T kk^T(kf-P) \quad (15)$$

Hence, combining Eqs. (14) and (15), Eq. (10) is being replaced by

$$\begin{aligned}(z-f)^T \nabla H(f) &+ \frac{1}{2}\lambda\|z-f\|_2^2 \\ &= \left(-\frac{1}{\lambda}k^T(kf-P)\right)^T k^T(kf-P) + \frac{1}{2\lambda}(kf-P)^T kk^T(kf-P) \\ &= (kf-P)^T A(kf-P) \\ &= \|kf-P\|_A \end{aligned} \quad (16)$$

where $A = -(1/2\lambda)kk^T$. The results follow. □

When the matrix $A = -(1/2\lambda)kk^T$, the term $(z-f)^T\nabla H(f) + (1/2)\lambda\|z-f\|_2^2$ can be rewritten as $\|kf-P\|_A$.

By comparing Eqs. (10) and (16), we use the weighted matrix A in the data fitting term of Eq. (16) instead of the Euclidean norm in that of Eq. (10). Namely, we introduced the least-squares combined with the weight norm to the data fitting term in Eq. (10). From Eq. (16), we can find that when A is equal to the identity matrix I, the weight data fitting term is the same as $\|kf-P\|_2^2$.

In this paper, the iterative algorithm was used to solve the proposed program in the alternating manner. In the ith iteration, the update z_i and f_i are obtained by minimising Eqs. (10) and (11) in the alternating manner, respectively:

$$z^i = \arg\min (z^i - f^{i-1})^T \nabla H(f^{i-1}) + \tfrac{1}{2}\lambda\|z^i - f^{i-1}\|_2^2 \quad (17)$$

$$f^i = \arg\min \tfrac{1}{2}\|z^i - f^i\|_2^2 + \mu\|z^i\|_{TV} \quad (18)$$

The above alternating minimisation algorithm computes an iterated sequence by starting from an initial value f^0

$$f^0, z^1, f^1, z^2, f^2, z^3, f^3, \ldots, z^i, f^i, \ldots$$

Hence, Eqs. (10) and (11) can be transformed as

$$S_h(f^{i-1}) : = z^i = \arg\min(z^i - f^{i-1})^T \nabla H(f^{i-1}) + \tfrac{1}{2}\lambda ||z^i - f^{i-1}||_2^2 \quad (19)$$

$$S_{tv}(z^i) : = f^i = \arg\min \tfrac{1}{2}||z^i - f^i||_2^2 + \mu ||z^i||_{TV} \quad (20)$$

For simplicity, Eqs. (19) and (20) can be reduced as

$$f^i = S_{tv}(S_h(f^{i-1})) = T(f^{i-1}) \quad (21)$$

where the operator $T = S_{tv}(S_h(\cdot))$ $T = S_{tv}(S_h(\cdot))$. In order to prove the existence and uniqueness of minimisers of the alternating algorithm, we very briefly review some basic definitions of convex, proper, lower semi-continuous, coercive function (see Appendix A). Convex, proper, lower semi-continuous, coercive function play a key role in optimisation. It is clear that $\|\cdot\|_{TV}$ is convex, lower semi-continuous, and proper [30,31]. The existence and uniqueness of minimisers of (21) are addressed in the following propositions, the proofs of which can be found in Appendix B.

Proposition 2. Let φ be convex and semi-continuous and $a > 0$. Suppose $x'$is defined as follows:

$$x' = \arg\min_x \|y - x\|_2^2 + a\phi(x). \quad (22)$$

Define S such that $x' = S(y)$for each y, Then S is firmly nonexpansive.

Proof. see [32, Lemma 2.4]. □

Proposition 3. *When $\lambda = k^T k + \varepsilon I$, the operator T in Eq. (21) is nonexpansive (where ε is small positive constant and I denotes identity matrix).*

Proof. See Appendix B, Proposition 3. □

Proposition 4. *Let $\{f^i\}$ be generated by Eq. (18), and then $\sum_{i=1}^{\infty} ||f^{i-1} - f^i||_2^2$ converge.*

Proof. See Appendix B, Proposition 4. □

Proposition 5. *For any initial value f^0, suppose sequence $\{f^i\}$ is generated by Eq. (21), then*

$$\lim_{i\to\infty} \|f^{i+1} - f^i\|_2 = \lim_{i\to\infty} \|T^{i+1}(f^0) - T^i(f^0)\| = 0 \quad (23)$$

Proof. See Appendix B, Proposition 5. □

According to Proposition 5, uniqueness of minimisers of the alternating algorithm was proved. Now we will prove the minimum of Eq. (21) is nonempty and compact.

Proposition 6. *Let g be coercive, semi-continuous, and proper function, and then the set of minima of $\arg\min_x g(x)$ is nonempty.*

Proof. The proof of Proposition 6 can be found in [33, Proposition 2.1.1]. □

Since the operator T of Eq. (21) is convex, semi-continuous, and proper, the condition that T is coercive states the minima of Eq. (21) is nonempty according to Proposition 5. Now, we will prove that T is coercive under certain conditions.

Let z be the reconstructed image, $|\nabla_1 z|_{s,t} = \sqrt{(z_{s,t} - z_{s-1,t})^2}$, $|\nabla_2 z|_{s,t} = \sqrt{(z_{s,t} - z_{s,t-1})^2}$. where s and t are the horizontal and vertical position of image z. We can obtain

$$\sum_{s,t} |(\nabla_1 z)|_{s,t} = \sum_{s,t} \sqrt{(z_{s,t} - z_{s-1,t})^2} = \|L_h z\|_1$$

$$\sum_{s,t} |(\nabla_2 z)|_{s,t} = \sum_{s,t} \sqrt{(z_{s,t} - z_{s,t-1})^2} = \|L_v z\|_1$$

where L_h and L_v are one-sided difference matrix in the horizontal direction and the vertical direction.

Proposition 7. *Let L_h and L_v be one-sided difference matrix in the horizontal direction and the vertical direction, respectively. And the matrix L is composed of L_h and L_v, which is defined as*

$$L = \begin{pmatrix} L_h \\ L_v \end{pmatrix}$$

When $Null\left(\sqrt{(1/2\lambda)}kk^T k\right) \cap Null\left((\eta/\sqrt{2})L\right) = \emptyset$, the operator T is coercive, where $Null(\cdot)$ denotes the null space of the corresponding matrix.

Proof. see Appendix B. □

If $f \in Null\left(\frac{\eta}{\sqrt{2}}L\right)$, any entry f_{ij} in the vector f is equal to a nonzero constant for any i and any j. Since the nonzero entries of the system matrix k is positive, $\sqrt{(1/2\lambda)}kk^T k$ is a nonzero vector. It follows that the condition $Null\left(\sqrt{(1/2\lambda)}kk^T k\right) \cap Null\left((\eta/\sqrt{2})L\right) = \emptyset$ holds in general. Since the operator T is coercive, the set of minima of $T(f,z)$ is nonempty. Suppose that $(f'\ z')$ is a minimiser of $T(f',z')$, and T is convex. Therefore, we have

$$\begin{bmatrix} \dfrac{\partial S_h(f^i)}{\partial f} \\ \dfrac{\partial S_{tv}(z^i)}{\partial z} \end{bmatrix} = \begin{pmatrix} 0 \\ 0 \end{pmatrix} \quad (24)$$

It implies that

$$\begin{cases} S_h(f') : = z' = \arg\min(z' - f')^T \nabla H(f') + \dfrac{1}{2}\lambda \|z' - f'\|_2^2 \\ S_{tv}(z') : = f' = \arg\min \dfrac{1}{2}\|z' - f'\|_2^2 + \mu \|z'\|_{TV} \end{cases} \quad (25)$$

Therefore, we have

$$f' = S_{tv}(S_h(f')) = T(f') \quad (26)$$

According to Propositions 5 and 7, the minima of Eq. (19) is nonempty and unique.

4. The alternating algorithm for limited angle tomography

We now describe the iterative steps of our algorithm, which solves the vector f for the optimisation program described in Eqs. (10) and (11), for the limited angle tomography. According to Eq. (24), z_i in Eq. (27) and f_i in Eq. (28) are alternately updated by minimising Eqs. (10) and (11) in the ith iteration:

$$z^i = f^{i-1} - \frac{1}{\lambda}\nabla H(f^{i-1}) = f^{i-1} - \frac{1}{\lambda}k^T(kf^{i-1} - P) \quad (27)$$

$$f^i = z^i + \mu \frac{\partial \|z^i\|_{TV}}{\partial z} \quad (28)$$

Because the image function is non-negative, we use f^i to denote the image estimate after projection onto the non-negative half-plane in the ith iteration. The image estimate f^i is a vector of length N with individual elements f_j^i, $j = 1,2,\ldots,N$. N is the number

of pixels in the reconstructed image:

$$f_j^i = \begin{cases} f_j^i, & f_j^i \geq 0, \\ 0, & f_j^i < 0, \end{cases} \quad j = 1,2,\ldots,N \tag{29}$$

The alternating iterative algorithm of Eqs. (27) and (28) computes an iterated sequence by staring from an initial value $f^0=0$. Each alternating iteration consists of two steps: the data-step in Eq. (27) and the TV-step in Eq. (28). The data-step enforce consistency with the projection data. The TV-step in Eq. (27) reduces the TV of the estimated image and handles data very well. The proposed algorithm alternates one iteration of data-step with TV-step. The overall iteration number is labeled by n, and the sub-iterations of the data-step and the TV-step are labeled by m and j, respectively. The symbols below are presented in the nth iteration. $f^{SD}[n,m]$ denotes the estimated image of mth data-step sub-iteration. $z^{pos}[n,m]$ denotes the mth estimated image after projection onto the non-negative half-plane. Finally, the estimated vector $z^{TV}[n,j]$ represents the estimated image of the jth TV-step sub-iteration. The steps of the algorithm are:

(1) Initialisation:

$$f^{SD}[n,0]=0, \quad n=0, B=20$$

(2) The data-step iteration, for $m=1,2,3,\ldots,M$ (M is the number of X-ray integrals):

$$z^{SD}[n,m] = f^{SD}[n,m-1] - \frac{1}{\lambda}\nabla H(f^{SD}[n,m-1])$$
$$= f^{SD}[n,m-1] - \frac{1}{\lambda}k'(kf^{SD}[n,m-1]-P)$$

where $\lambda = k'k+\varepsilon I$, $\varepsilon = 10^{-8}$, and k' is the transpose of the vectors k described in Section 3.

(3) Positivity constraint:

$$z_j^{POS}[n] = \begin{cases} z_j^{SD}[n,M], & z_j^{SD}[n,M] \geq 0, \\ 0, & z_j^{SD}[n,M] < 0, \end{cases} \quad j = 1,2,\ldots,N$$

The image estimate $z^{SD}[n,M]$ is a vector of length N with individual elements $z_j^{SD}[n,M]$ and N the number of pixels in the reconstructed image.

(4) TV-step initialisation:

$$z^{TV}[n,1] = z^{POS}[n]$$

$$\beta = -\|z^{SD}[n]-z^{POS}[n]\|_2$$

The image estimate $z^{POS}[n]$ is a vector of length N with individual elements $z_j^{POS}[n]$.

(5) TV-step iteration, for $j=2,3,\ldots,B$ (B is the number of sub-iteration):

$$R_{s,t}[n,j-1] = \frac{\partial \|z^{TV}\|_{TV}}{\partial z_{s,t}}\bigg|_{z_{s,t}=z^{TV}[n,j-1]}$$

$$R[n,j-1] = \frac{R[n,j-1]}{|R[n,j-1]|}$$

$$z^{TV}[n,j] = z^{TV}[n,j-1] + \mu\beta R[n,j-1]$$

where the step size $\mu = 0.2$.

(6) Initialise next loop:

$$f^{SD}[n+1,1] = z^{TV}[n,L]$$

Increment n and return to step (2).

5. Experimental results

For inverse problems, numerical tests of reconstruction methods usually make use of simulated data from the numerical solution of the forward problem. One typical issue is coined as the inverse crimes [35]. It is possible that the essential ill-posedness of the inverse problem may not be evident. This happens especially when the projection data are generated by applying the projection system matrix to a discrete image. Hence, the results could be overly optimistic and unreliable. One approach to avoid the inverse crime is that the discrete image entails mismatch with projection data in the forward and the inverse process. In this case, the data model is more realistic in that the projection data are generated by computing line integrals through computer phantom represented by continuous function [35]. Hence, to verify the performance of the method introduced above, we make two sets of studies. The proposed algorithm is implemented in a MATLAB 6.5™ environment on a desktop computer (2.67 GHz core(TM) 2 Quad with 2.5 GB random access memory) to test the performance using the simulated Shepp–Logan phantom and a real bee phantom as the test images.

In the first set of studies, the projection data are generated by computing line integrals through Shepp–Logan phantom defined as combinations of analytic shapes such as ellipsoids and cylinders. In this case, the discrete image entails mismatch with projection data generated from continuous objection. Hence, there exists no image f that satisfies data model $kf=P$. In the second set of studies, the proposed method is tested using real projection data obtained from the Institute of High Energy Physics Chinese Academy of Sciences. And we compare the proposed method with the method in [29] and standard expectation maximisation (EM) algorithm which has been widely applied to solving the under-determined linear systems in tomographic imaging.

In the first sets of studies, the simulated projection data are generated by computing line integrals through $128\times128\times128$ realistic phantom represented by continuous function. For the results in this section, we demonstrate and validate our algorithm under "ideal" and "noisy" conditions in order to verify the effectiveness of the proposed algorithm. For the image reconstruction from projections of the continuous Shepp–Logan phantom, the simulated detector now has 99×300 bins and the image size is reconstructed into 128^3 array. We define the scanning angle by taking 20 angular samples uniformly distributed over an angular range of 20°. The imaging parameters of the typical scanner geometry are defined as

(1) The distance from the X-ray source to the centre of reconstructed image is 400 mm.
(2) The distance from the X-ray source to the detector is 800 mm.
(3) The projection interval is 1°.
(4) The reconstruction matrix is $128\times128\times128$.
(5) The pixel matrix of the detector was 99×300.
(6) The pixel pitch of the detector is 0.50647 mm.
(7) The pixel pitch of the object is 0.3125 mm.

The original mid-plane slice of the Shepp–Logan phantom is shown in Fig. 2(a). The display gray scale is [0,255]. In this study, the number of iterations for the proposed algorithm is 30, while the method in [29] and EM algorithm are 50, respectively. We define the scanning angular range of 20° in which the projection data at 20 uniformly distributed views are available. Fig. 2 (b) shows that the mid-plane image is reconstructed by using our method from 20 noiseless projection data. Fig. 2(c, d) shows the reconstructed images by using the method in [29] and EM algorithm in the same situation, respectively. In the second

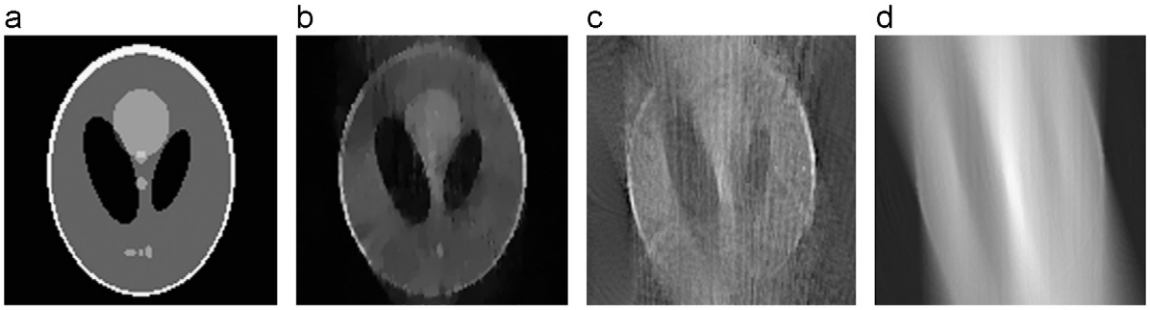

Fig. 2. The 128×128 Shepp–Logan image reconstruction with noiseless projections which are available in angular range 20°. (a) The original mid-plane image, (b) reconstruction using our method, (c) reconstruction using the method in [29], and (d) reconstruction using the EM method.

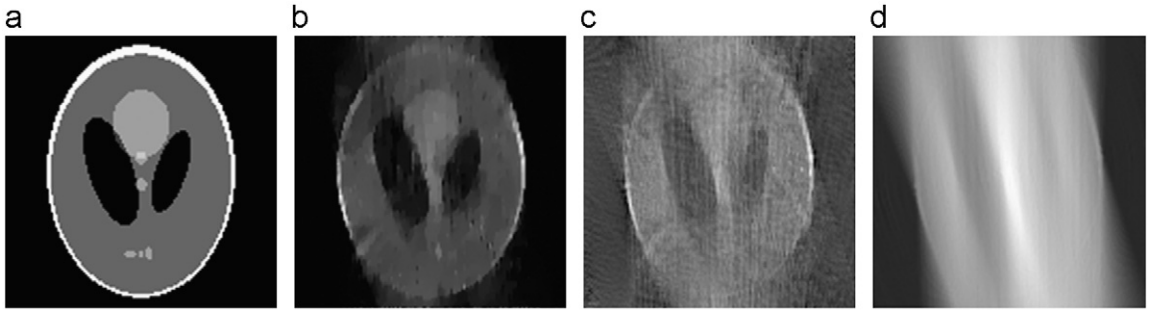

Fig. 3. The 128×128 Shepp–Logan image reconstruction with noisy projections which are available in angular range 20°. (a) The original mid-plane image, (b) reconstruction using our method, (c) reconstruction using the method in [29], and (d) reconstruction using EM method.

simulation, additive Gaussian noise with standard deviation 3% of the maximum value of the generated projection is added to the projection data, leading to a peak-signal-to-noise ratio (PSNR) of 21.452 dB. Fig. 3 (b) shows the mid-plane images reconstructed by using our method with the noisy projection data. Fig. 3(c, d) shows the reconstructed images by using the method in [29] and EM algorithm in the same situation, respectively. It can be seen that Figs. 2(b) and 3(b) contain a tiny deviation from the original phantom. On the other hand, Figs. 2 (c, d) and 3 (c, d) are much distorted. It is shown in Fig. 2(c, d) that the reconstructed images suffer from the different artifacts in image reconstruction compared to our method in the "ideal" condition. Moreover, the reconstructed image by using our method has a high contrast and are clearer than those by using the other algorithms in the same situation. Compared to the other algorithms, the image reconstructed by our method displays better results in "noisy" condition as shown in Fig. 3. To further confirm this observation, we have compared the profiles along the central lines of the image Fig. 2 to Fig. 3 in the horizontal and vertical directions, shown in Fig. 4. The numerical results of the two methods are summarised in Table 1 and 2. Table 1 contains the computation times of the reconstructions when the mid-plane image is reconstructed by using different methods from the noiseless projection data. The computation times of the reconstructions is tabulated in Table 2 when the mid-plane image is reconstructed by using different methods from the noisy projection data. From Tables 1 and 2, it is obvious that the proposed algorithm requires less running time than the method in [29] and the EM algorithm.

In the second studies, the projection data are generated from realistic bee projection data at 90^0 views (provided by the Institute of High Energy Physics Chinese Academy of Sciences). And its imaging parameters of the typical scanner geometry are defined as

(1) The distance from the X-ray source to the centre of reconstructed image is 306 mm.
(2) The distance from the X-ray source to the detector is 351 mm.
(3) The reconstruction matrix is $128 \times 128 \times 128$.
(4) The pixel pitch of the object is 0.0535 mm.

The detector employed an X-ray FDI-18 mm camera system (Photonic Science Ltd.) with 1300×1030 array elements and 10.9×10.9 μm per element. The detector at each view contains 1300×1030 bins, of which the data 1300×963 have been employed in the experiments. The projection of the bee phantom at a given angle is shown in Fig. 5(a). The number of iterations for the proposed algorithm is 30. And the number of iterations for the method in [29] and EM algorithm are 50. Fig. 5(b–d) presents a comparison among the various reconstructions from the limited angle data which consisted of 18 projections with total opening angle of 90° (5°steps). Fig. 5(b) presents that the plane is reconstructed by using FBP algorithm with 360 projection data generated from a total view angle of 180° (0.5°steps). In FBP reconstructions we reduce the effects of noise by applying the Ram-Lak filter multiplied by the Hamming window to the filtering in the frequency domain and use the nearest neighbor interpolation. Fig. 5(c) shows that the plane reconstructed image is presented by using our algorithm. Fig. 5(d, e) shows the reconstructed images by using the method in [29] and EM algorithm in the same situation, respectively. Although the reconstructed images in Fig. 5(c) suffer from different artifacts, it has a high contrast and more clear reconstructions compared to Fig. 5(d, e). In a real image reconstruction topic, however, the reference image is not available, and a no-reference or "blind quality assessment" approach is desirable. Hence real images are ultimately to be viewed by human beings, the only "correct" method of quantifying visual image quality

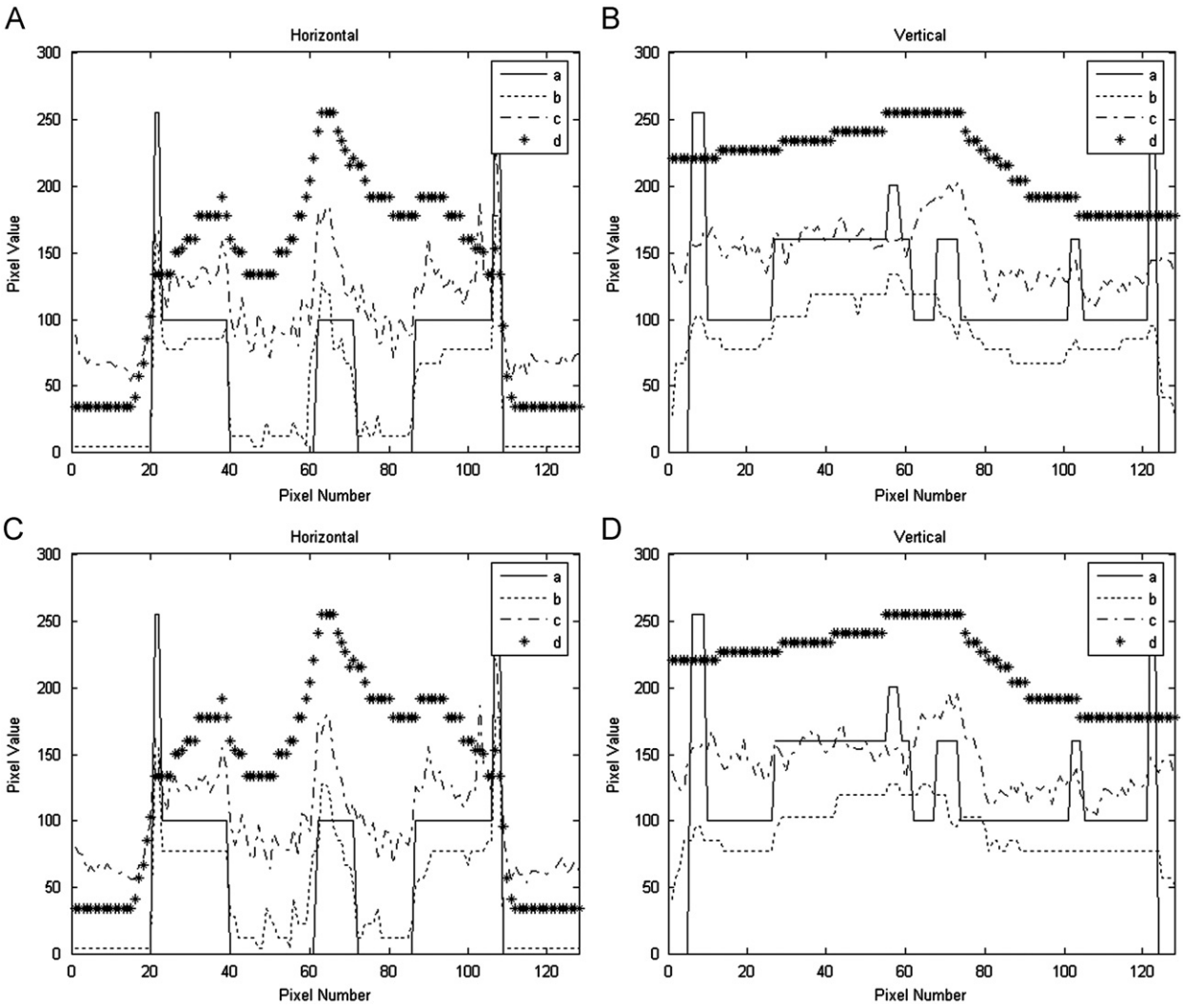

Fig. 4. The comparison of images profile. (A) Image profiles along the centres of the images in the horizontal direction obtained from Fig. 2(a, solid line), Fig. 1(b, dotted line), Fig. 2(c, dashdot line), and Fig. 2(d, dashed line). (B) Image profiles along the centres of the images in the vertical direction obtained from Fig. 2(a, solid line), Fig. 2(b, dotted line), Fig. 2(c, dashdot line), and Fig. 2(d, dashed line). (C) Image profiles along the centres of the images in the horizontal direction obtained from Fig. 3(a, solid line), Fig. 3(b, dotted line), Fig. 3(c, dashdot line), and Fig. 3(d, dashed line). (D) Image profiles along the centres of the images in the vertical direction obtained from Fig. 3(a, solid line), Fig. 3(b, dotted line), Fig. 3(c, dashdot line), and Fig. 3(d, dashed line).

Table 1
Computation times of the limited angle reconstructions given in Fig. 2.

	New method (times, s)	The method in [31] (times, s)	EM (times, s)
Computation time	475.462	769.351	808.905

Table 2
Computation times of the limited angle reconstructions given in Fig. 3.

	New method (times, s)	The method in [31] (times, s)	EM (times, s)
Computation time	484.678(s)	776.295(s)	814.943(s)

is through subjective evaluation. In this experiment, the reconstructed image by using FBP algorithm is assumed to be reference image. To further confirm this observation, we have compared the profiles along the central lines of the images in Fig. 5 in the horizontal and vertical directions, shown in Fig. 6. The corresponding reference profiles are also displayed as the thin lines.

6. Conclusion

In this paper, we have proposed a new alternating optimisation program for the reconstruction of object in limited angle tomography. The performances in terms of image quality have been shown in the previous sections in "ideal", "noisy", and "real" conditions. In general, the comparable image quality performance between the proposed algorithm and other algorithms is that the proposed algorithm has a very positive effect on the quality of reconstruction. We have employed an alternating minimisation algorithm to solve the proposed minimisation problem. Numerical experiments show that the proposed method is robust and effective. Future efforts will focus on developing more efficient algorithm that can offer real time reconstruction with good image quality.

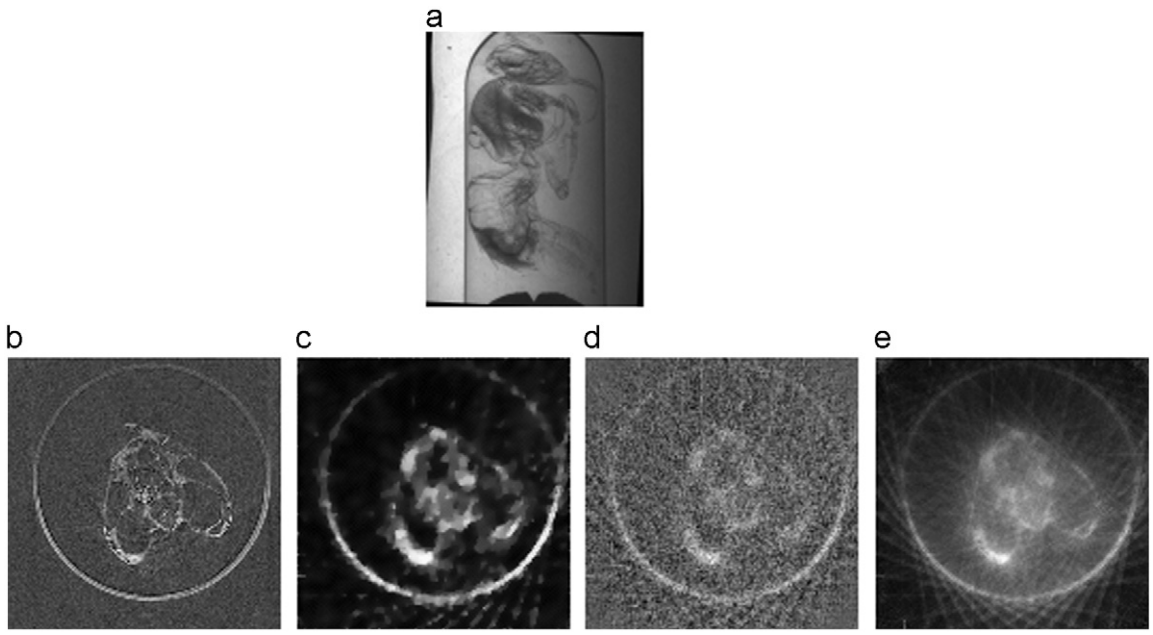

Fig. 5. Reconstructions along vertical slice through the real bee phantom. (a) Projection radiography of the bee phantom, (b) reconstruction using the FBP method, (c) reconstruction using our method, (d) reconstruction using the method in [29] and (e) reconstruction using the EM method.

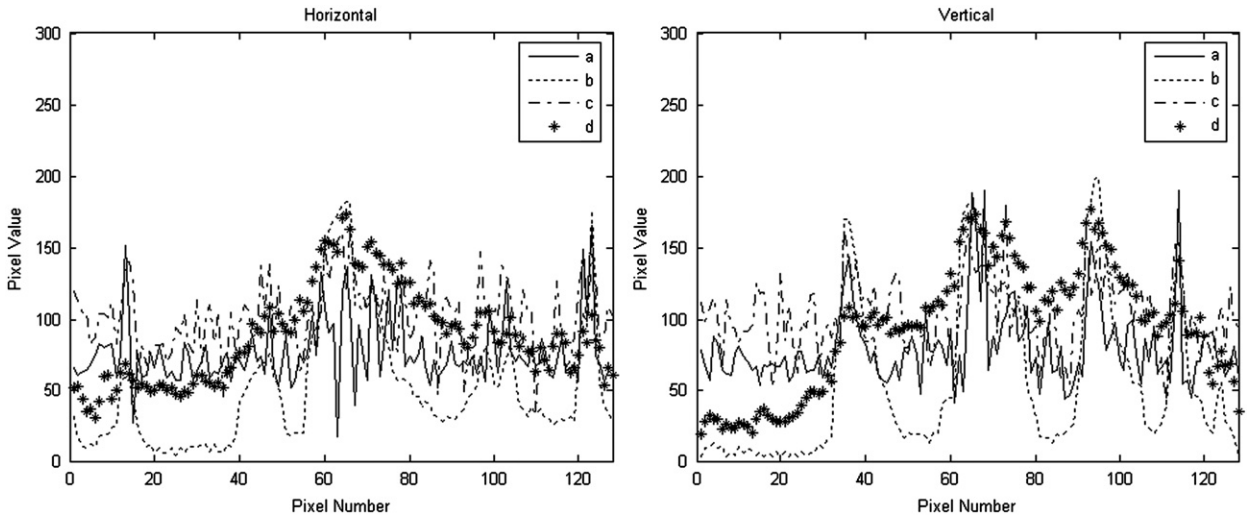

Fig. 6. The comparison of images profile. (A) Image profiles along the centres of the images in the horizontal direction obtained from Fig. 5(b, solid line), Fig. 5(c, dotted line), Fig. 5(d, dashdot line), and Fig. 5(e, dashed line). (B) Image profiles along the centres of the images in the vertical direction obtained from Fig. 5(b, solid line), Fig. 5(c, dotted line), Fig. 5(d, dashdot line), and Fig. 5(e, dashed line).

Acknowledgment

This work is supported by the National Basic Research Program of China (973 Program) (Grant No. 2011CB707104), Ministry of Education of the People's Republic of China (Grant No. 107032) and Liaoning Excellent Talent Funding, and the National Natural Science Foundation of China (Grant No. 61072093).

Appendix A

Consider a function f: $X\rightarrow[-\infty,+\infty]$, and X is a real Hilbert space.

Definition 1. The function f is convex if $f(ax+(1-a)x)\leq af(x)+(1-a)f(x)$, for any x and any $a\in[0,1]$.

Definition 2. The function f is proper if $f(x)<\infty$, for at least one $x\in X$, and $f(x)>-\infty$, for all $x\in X$.

Definition 3. f is lower semi-continuous at y if

$$\lim_{\delta\rightarrow 0}\inf_{x\in B(y,\delta)} f(x)\geq f(y)$$

where $B(y,\delta)=\{x:||x-y||\leq\delta\}$ is the δ-ball around y and $\|\cdot\|$ is the norm in the Hilbert space.

Definition 4. f is called coercive if it verifies $\lim_{\|x\|\rightarrow\infty} f(x)=\infty$.

Definition 5. f is called nonexpansive if, for any $x_1, x_2\in R$, we have

$$\|f(x_1)-f(x_2)\|_2\leq\|x_1-x_2\|_2$$

Appendix B

Proposition 3. *When $\lambda=k^Tk+\varepsilon I$, the operator T in Eq. (19) is nonexpansive (where ε is small positive constant and I denote identity matrix).*

Proof. With Proposition 2, we know that S_{tv} of Eq. (19) is nonexpansive, and, for any x and y, we have

$$\begin{aligned}\|T(x)-T(y)\|_2 &= \|S_{tv}(S_h(x))-S_{tv}(S_h(y))\|_2 \le \|S_h(x)-S_h(y)\| \\ &= \|x-\frac{1}{\lambda}\nabla H(x)-y+\frac{1}{\lambda}\nabla H(y)\|_2 \\ &= \|x-y+\frac{1}{\lambda}k^Tk(x-y)\|_2 \\ &= \|\left(1-\frac{1}{\lambda}k^Tk\right)(x-y)\|_2 \\ &= \|\frac{\varepsilon I}{k^Tk+\varepsilon I}\|_2\|x-y\|_2 \\ &= \|x-y\|_2 \end{aligned} \tag{B.1}$$

The result follows. □

Proposition 4. *Let $\{f^i\}$ be generated by Eq. (18), and then $\sum_{i=1}^{\infty}\|f^{i-1}-f^i\|_2^2$ converge.*

Proof. We consider the Taylor series expansion of $S_h(f^i,z)$ in the second variable and set $z=z^i$ in the calculation, and we have

$$\begin{aligned}S_h(f^i,z^i) \approx S_h(f^i,z^{i+1})-(z^i-z^{i+1})^T\frac{\partial S_h(f^i,z^{i+1})}{\partial z} \\ +\frac{1}{2}(z^i-z^{i+1})^T\frac{\partial^2 S_h(f^i,z^{i+1})}{\partial z^2}(z^i-z^{i+1})\end{aligned} \tag{B.2}$$

Since z^{i+1} is the minimiser of $S_h(f^i,z)$, we have

$$\frac{\partial S_h(f^i,z^{i+1})}{\partial z}=0 \tag{B.3}$$

And the derivative of Eq. (B.3) can be obtained as

$$\frac{\partial^2 S_h(f^i,z^{i+1})}{\partial z^2}=\lambda=k^Tk+\varepsilon I \tag{B.4}$$

Because $k^Tk+\varepsilon I$ is symmetric, positive definite and its eigenvalues are larger than ε, Eq. (B.2) can be rewritten as (by considering Eqs. (B.3) and (B.4))

$$S_h(f^i,z^i)-S_h(f^i,z^{i+1}) \ge \varepsilon\|z^i-z^{i+1}\|_2^2 \tag{B.5}$$

Since $S_h(f^{i+1},z^{i+1}) \le S_h(f^i,z^{i+1})$, we have

$$S_h(f^i,z^i)-S_h(f^{i+1}.z^{i+1}) \ge S_h(f^i,z^i)-S_h(f^i,z^{i+1}) \ge \varepsilon\|z^i-z^{i+1}\|_2^2 \tag{B.6}$$

Since the operator S_{tv} is nonexpansive, we can obtain

$$\|z^i-z^{i+1}\|_2^2 \ge S_{tv}(z^i)-S_{tv}(z^{i+1})=\|f^i-f^{i+1}\|_2^2 \tag{B.7}$$

Considering Eqs. (B.6) and (B.7), we have

$$S_h(f^i,z^i)-S_h(f^{i+1}.z^{i+1}) \ge \varepsilon\|f^i-f^{i+1}\|_2^2 \tag{B.8}$$

It follows that $\sum_{i=0}^{\infty}\|f^i-f^{i+1}\|_2^2$ is bounded, and $\sum_{i=0}^{\infty}\|f^i-f^{i+1}\|_2^2$ converges. □

Proposition 5. *For any initial value f^0, suppose sequence $\{f^i\}$ is generated by Eq. (21), then*

$$\lim_{i\to\infty}\|f^{i+1}-f^i\|_2=\lim_{i\to\infty}\|T^{i+1}(f^0)-T^i(f^0)\|=0 \tag{B.9}$$

Proof. Since $\sum_{i=0}^{\infty}\|f^i-f^{i+1}\|_2^2$ converges, we have

$\lim_{i\to\infty}\|f^{i+1}-f^i\|_2=\lim_{i\to\infty}\|T^{i+1}(f^0)-T^i(f^0)\|=0$ □

Proposition 7. *Let L_h and L_v be one-sided difference matrix in the horizontal direction and the vertical direction, respectively. And let L be*

$$L=\begin{pmatrix}L_h\\ L_v\end{pmatrix}$$

When $Null\left(\sqrt{(1/2\lambda)}kk^Tk\right)\cap Null\left((\eta/\sqrt{2})L\right)=\emptyset$, the operator T is coercive, where $Null(\cdot)$ denotes the null space of the corresponding matrix.

Proof. The lower bound of the discrete total variation is given by

$$\begin{aligned}||z||_{TV} &= \sum_{s,t}|\nabla z_{s,t}| = \sum_{s,t}\sqrt{(z_{s,t}-z_{s-1,t})^2+(z_{s,t}-z_{s,t-1})^2} \\ &\ge \frac{1}{\sqrt{2}}\sum_{s,t}|(\nabla z)|_{s,t}+|(\nabla z)|_{s,t} \\ &= \frac{1}{\sqrt{2}}\|Lz\|_1\end{aligned} \tag{B.10}$$

According to the Lambda principle, Eqs. (9) and (10) can be rewritten as

$$T(f,z)=(z-f)^T\nabla H(f)+\tfrac{1}{2}\lambda\|z-f\|_2^2+\eta\|z\|_{TV} \tag{B.11}$$

where η is a positive constant. Considering inequality (B.10) and Eq. (B.11), we have

$$\begin{aligned}T(f,z) &= (z-f)^T\nabla H(f)+\frac{1}{2}\lambda\|z-f\|_2^2+\eta\|z\|_{TV} \\ &\ge \left(-\frac{1}{\lambda}k^T(kf-P)\right)^Tk^T(kf-P) \\ &\quad +\frac{1}{2\lambda}(kf-P)^Tkk^T(kf-P)+\frac{\eta}{\sqrt{2}}\|Lz\|_1 \\ &= -\frac{1}{2\lambda}(kf-P)^Tkk^T(kf-P)+\frac{\eta}{\sqrt{2}}\|Lz\|_1 \\ &= -\frac{1}{2\lambda}kk^T\|kf-P\|_2^2+\frac{\eta}{\sqrt{2}}\|Lz\|_1\end{aligned} \tag{B.12}$$

$$T(f,z)\ge -\left\|\left[\sqrt{\frac{1}{2\lambda}kk^T}\,k0\right]\begin{bmatrix}f\\ z\end{bmatrix}-\left[\sqrt{\frac{1}{2\lambda}kk^T}\,P0\right]\right\|_2^2+\frac{\eta}{\sqrt{2}}\left\|\begin{pmatrix}0 & L\end{pmatrix}\begin{pmatrix}f\\ z\end{pmatrix}\right\|_1 \tag{B.13}$$

where 0 is the zero vector. Let

$$\begin{pmatrix}m\\ n\end{pmatrix}=\left[\sqrt{\frac{1}{2\lambda}kk^T}\,k,0,\frac{\eta}{\sqrt{2}}L\right]\begin{bmatrix}f\\ z\end{bmatrix} \tag{B.14}$$

when the condition $Null\left(\sqrt{(1/2\lambda)}kk^Tk\right)\cap Null\left((\eta/\sqrt{2})L\right)=\emptyset$ and $\left\|\begin{matrix}f\\ z\end{matrix}\right\|_2^2$ tends to infinity, either $\|m\|_2^2$ or $\|n\|_2^2$ tends to infinity. Therefore, $T(f)$ also tends to infinity according to Eq. (B.13). The result follows. □

References

[1] F. Natterer, in: The Mathematics of Computerized Tomography, John Wiley & Sons Ltd, Chichester, 1986.
[2] E.Y. Sidky, C.M. Kao, X. Pan, Accurate image reconstruction from few-views and limited-angle data in divergent beam CT, J. X-Ray Sci. Technol. 14 (2) (2006) 119–139.
[3] H.H. Barrett, K.J. Myers, in: Foundations of Image Science, John Wiley & Sons, Inc., Hoboken, NJ, 2004.
[4] J.S. Kole, Statistical image reconstruction for transmission tomography using relaxed ordered subset algorithms, Phys. Med. Biol. 50 (2005) 1533–1545.
[5] S. Siltanen, V. Kolehmainen, S. Järvenpää, J.P. Kaipio, P. Koistinen, M. Lassas, J. Pirttilä, E. Somersalo, Statistical inversion for medical X-ray tomography with few radiographs I: general theory, Phys. Med. Biol. 48 (2003) 1437–1463.
[6] K.M. Hanson, G.W. Wecksung, Bayesian approach to limited angle reconstruction in computed tomography, J. Opt. Soc. Am. 73 (1983) 1501–1509.
[7] K. Sauer, J. Sachs Jr., K. Klifa, Bayesian estimation of 3-D objects from few radiographs, IEEE Trans. Nucl. Sci. 41 (5) (1994) 1780–1790.
[8] V. Kolehmainen, S. Siltanen, S. Järvenpää, J.P. Kaipio, P. Koistinen, M. Lassas, J. Pirttilä, E. Somersalo, Statistical inversion for medical X-ray tomography with few radiographs II: application to dental radiology, Phys. Med. Biol. 48 (2003) 1465–1490.
[9] E.J. Candes, J.K. Romberg, Practical signal recovery from random projections, in: Computational Imaging III, Proceedings of the SPIE, vol. 5674, 2005.
[10] M. Rantala, S. Vänskä, S.ää Järvenp, M. Kalke, M. Lassas, J. Moberg, S. Siltanen, Wavelet-based reconstruction for limited angle X-ray tomography, IEEE Trans. Med. Imaging 25 (2006) 210–217.
[11] A.H. Andersen, Algebraic reconstruction in CT from limited views, IEEE Trans. Med. Imaging 8 (1989) 50–55.
[12] C. Byrne, Block-iterative interior point optimisation methods for image reconstruction from limited data, Inverse Probl. 16 (2000) 1405–1419.
[13] C. Popa, R. Zdunek Kaczmarz, Extended algorithm for tomographic image reconstruction from limited data, Math. Comput. Simulation 65 (2004) 579–598.
[14] J.L. Prince, A.S. Willsky, Constrained sinogram restoration for limited-angle tomography, Opt. Eng. 29 (1990) 535–544.
[15] H. Kudo, T. Saito, Sinogram recovery with the method of convex projections for limited data reconstruction in computed tomography, J. Opt. Soc. Am. A 8 (1991) 1148–1160.
[16] M.C. Lawrence, M.A. Jaffer, B.T. Sewell, The application of the maximum entropy method to electron microscopic tomography, Ultramicroscopy 31 (1989) 285–301.
[17] R.T. Smith, C.K. Zoltani, G.J. Klem, M.W. Coleman, Reconstruction of tomographic images from sparse data sets by a new finite element maximum entropy approach, Appl. Opt. 30 (1991) 573–582.
[18] M.L. Reis, N.C. Roberty, Maximum entropy algorithms for image reconstruction from projections, Inverse Probl. 8 (1992) 623–644.
[19] V. Kolehmainen, M. Lassas, S. Siltanen, Limited data X-ray tomography using nonlinear evolution equations, SIAM J. Sci. Comput. 30 (3) (2008) 1413–1429.
[20] P. Milanfar, W.C. Karl, A.S. Willsky, A moment-based variational approach to tomographic reconstruction, IEEE Trans. Med. Imaging 5 (3) (1996) 459–470.
[21] C. Robert, New neural network algorithm for image reconstruction from fan-beam projections, Neurocomputing 72 (2009) 3238–3244.
[22] M. Persson, D. Bone, H. Elmqvist, Total variation norm for three dimensional iterative reconstruction in limited view angle tomography, Phys. Med. Biol. 46 (2001) 853–866.
[23] E. Candes, J. Romberg, T. Tao, Robust uncertainty principles: exact signal reconstruction from highly incomplete frequency information, IEEE Trans. Inform. Theory 52 (2006) 489–509.
[24] Y. Sidky Emil, Xiaochuan Pan, Image reconstruction in circular cone-beam computed tomography by constrained total variation minimisation, Phys. Med. Biol. 53 (17) (2008) 4777–4807.
[25] Xiaochuan Pan Yu Zou, Exact image reconstruction on pi-lines from minimum data in helical cone-beam CT, Phys. Med. Biol. 49 (6) (2006) 941–959.
[26] Xiaochuan Pan Yu Zou, Y. Sidky Emil, Image reconstruction in regions-of-interest from truncated projections in a reduced fan-beam scan, Phys. Med. Biol. 50 (1) (2005) 13–27.
[27] J. Velikina, S. Leng, G.H. Chen, Limited view angle tomographic image reconstruction via total variation minimization, SPIE Med. Imaging 8 (2) (2007) 651020.1–651020.7.
[28] Y. Nesterov, Gradient methods for minimizing composite objective function, Centre for Operations Research and Econometrics (CORE), Catholic Univ. Louvain, Louvain-la-Neuve, Belgium, CORE Discussion Paper 2007/76, 2007.
[29] S.J. Wright, R.D. Nowak, M.A.T. Figueiredo, Sparse reconstruction by separable approximation, IEEE Trans. Signal Process. 57 (2009) 2479–2492.
[30] J. Bioucas-Dias, M. Figueiredo, A new TwIST: two-step iterative shrinkage/thresholding algorithms for image restoration, IEEE Trans. Image Process. 16 (12) (2007) 2992–3003.
[31] P.L. Combettes, V.R. Wajs, Signal recovery by proximal forward backward splitting, Multiscale Model. Simulation 4 (2005) 1168–1200.
[32] R.T. Rockafellar, R. Wets, in: Variational Analysis, Springer Verlag, Berlin, Germany, 1998.
[33] D. Bertsekas, A. Nedic, E. Ozdaglar, in: Convex Analysis and Optimisation, Athena Scientific, Belmont, MA, 2003.
[34] Lu. Xiao, Y. Sun, G. Bai, Adaptive wavelet-Galerkin methods for limited angle tomography, Image Vision Comput. 28 (4) (2010) 696–703.
[35] A.H. Delaney, Y. Bresler, Globally convergent edge preserving regularized reconstruction: an application to limited-angle tomography, IEEE. Trans. Imaging Proc. 7 (1998) 204–221.

Xiaoqiang Lu is currently pursuing his Ph.D. degree in the Department of Electrical Engineering at the Dalian University of Technology, Dalian, China. His research interests include cellular automata, inverse problem, and super resolution image reconstruction.

Yi Sun received her B.S. and M.S. degrees both in electrical engineering from the Dalian University of Technology, Dalian, China, in 1986 and 1989, respectively, and her Ph.D. degree in optical engineering from the same university in 2002. Since 1989, she has been with the department of electrical engineering, Dalian University of Technology, where she is currently a professor. Her research interests include new medical imaging modalities, reconstruction algorithms, and physical impacts on CT image. She received two awards from the Liaoning Government for her contribution to the X-ray image processing and cone-beam CT in 2004 and 2005, respectively, and the award from Chinese CT/MRI Society for new 3-D imaging development in China in 2006. She is both the IEEE member and SPIE member now.

Dr Yuan Yuan is currently a researcher at Xi'an Institute of Optics and Precision Mechanics, Chinese Academy of Sciences, China. She is interested in areas of visual information processing, compression, and content analysis.